Available online at www.sciencedirect.com
ScienceDirect
Journal of Catalysis 245 (2007) 133–143
JOURNAL OF CATALYSIS
www.elsevier.com/locate/jcat

Strained Pd overlayers on Ni nanoparticles supported on alumina and catalytic activity for buta-1,3-diene selective hydrogenation

R. Massard [a], D. Uzio [a], C. Thomazeau [a,*], C. Pichon [a], J.L. Rousset [b], J.C. Bertolini [b]

[a] *IFP, Solaize BP n°3, Lyon, BP3, F-69390 Vernaison cedex, France*
[b] *Institut de Recherches sur la Catalyse, CNRS, 2 av. Albert Einstein, F-69626 Villeurbanne cedex, France*

Received 21 June 2006; revised 11 September 2006; accepted 12 September 2006
Available online 30 October 2006

Abstract

To study the role of strain effects on catalytic properties in the case of supported particles, core–shell PdNi bimetallic nanoparticles were prepared by chemical synthesis and studied in hydrogenation of buta-1,3-diene. Multitechnique characterisation (EDS, TEM, EXAFS) results indicate good homogeneity of the bimetallic particles in terms of size and composition. The core–shell structure of NiPd bimetallic particles and the compressive stress induced on Pd atoms in the top layer due to its larger atomic radius compared with Ni, have been evidenced by EXAFS analyses. According to the literature, Pd activity for buta-1,3-diene hydrogenation is amplified when Pd is strained at the surface of Ni single crystal faces, mainly in the case of (110) planes. This compressive stress is supposed to produce surface reconstructions with undulated Pd row structures. In our case, no amplification of the Pd activity for buta-1,3-diene hydrogenation performed in liquid-phase conditions was observed for a monolayer of Pd strained on 5 nm Ni particles. Consequently, the compressive strain on the Pd atoms at the surface of the nanoparticles seems not to play a major role in the amplification of the activity for buta-1,3-diene hydrogenation. Surface reconstructions observed on extended surfaces to relax the surface stress seems to be the key point for Pd activity amplification. For supported particles, we propose that this relaxation phenomenon does not occur for such small three-dimensional particles.

Keywords: Bimetallic catalyst; Pd; Ni; Core–shell; Strain; Buta-1,3-diene hydrogenation

1. Introduction

In the field of heterogeneous catalysis, group VIII metals like Pd-, Pt-, or Ni-based catalysts are among the most active transition metals for selective hydrogenation of dienes. In this group of metals, Pd is more active and selective than Pt or Ni [1]. Over the last decades, many improvements were realised in the synthesis of heterogeneous catalysts with well designed structures. Indeed, new kinds of bimetallic catalysts exhibit improved catalytic properties for transition metals. Bimetallic catalysts can be split into two types: monometallic particles constituting each component on the same support and supported bimetallic particles. In the first case, co-operative phenomena will govern catalytic performance through an additive effect of the catalytic properties of both metals. New catalytic properties appear when two transition metals are in contact, which may be called synergetic properties. Depending on this association, these particular catalytic behaviours of bimetallic catalysts are usually described in terms of either an "ensemble effect" [2,3], associated with the number of surface atoms needed for the catalytic process to occur, or the so-called "ligand effect," associated with the electronic modifications induced by the system constituents. An additional "bi-site effect" [4] in which both components play a specific role with respect to the reactants of the catalytic reaction has also been suggested to explain synergetic effects on catalysis by alloys.

For alloys, the surface structure depends on the thermodynamics of the miscibility and segregation process of the two metals. Various types of structures can be obtained: a mixed solution of both metals, which we call "alloy," and a metal on metal deposit, called "overlayer system" [5]. In the case of PdNi extended surfaces considered as model catalysts, the surface develops a nearly Pd overlayer system when stabilised by

* Corresponding author. Fax: +33 4 78 02 20 66.
E-mail address: cecile.thomazeau@ifp.fr (C. Thomazeau).

0021-9517/$ – see front matter
doi:10.1016/j.jcat.2006.09.014

heating (segregation phenomenon), the Pd nominal bulk content being very low [6,7]. In that case, polycrystalline or oriented PdNi bulk alloys annealed at 600 °C have shown an increase of Pd catalytic activity for gas-phase buta-1,3-diene selective hydrogenation [8,9]. For instance, the activity of a $Pd_8Ni_{92}(110)$ alloy is 20 times higher than that measured for the Pd(110) monometallic model catalyst [9]. For such an alloy, the Pd surface composition of the PdNi alloy equilibrated at 600 °C is >80% (related to 8% Pd nominal concentration) [6,9]. Pd, which has a lower surface free energy than Ni, segregates to the surface to a great extent. Nevertheless, the second layer in the alloy is composed mainly by Ni (up to 80%) [6]. A first explanation for the increased activity of the surface Pd atoms could be an electronic effect induced by the Ni atoms located underneath the Pd surface atoms [10]. However, PdNi model catalysts prepared by Pd atom deposition on a Ni(110) crystal (evaporation under UHV) have shown increased catalytic activity for buta-1,3-diene selective hydrogenation as well, even when the Pd coverage is greater than one layer [1,5,11–13]. Thus, the catalytic activity of four layers of Pd deposited on Ni(110) is amplified by 40 with respect to pure Pd(110). This shows that Ni influences the properties of Pd surface atoms without being in contact with it. Keeping in mind that the Pd bulk lattice parameter is ∼10% larger than the Ni one, the Pd deposit on Ni suffers a compressive strain to adapt to the Ni bulk lattice. This Pd stress could be an alternative explanation for Pd activity amplification [1,14]. However, experimental and theoretical studies have shown that the Pd strain is partially relaxed by generating new surface structures in which some Pd surface atoms are slightly shifted out of their normal position in a fcc crystal arrangement, creating new kinds of active sites [14,15]. This has been demonstrated both for Pd/Ni(110) deposits and for $Pd_8Ni_{92}(110)$ alloy [1,9,16,17]. Therefore, the amplification of the catalytic activity measured for Pd surface atoms on pure Ni or for Ni-rich PdNi alloys could be the consequence of some compressive strain and/or unusual surface structures after partial relaxation [14].

Many studies have focused on the preparation and characterisation of supported core–shell NiPd particles [18–23]. NiPd nanoparticles were prepared in many different ways, including co-impregnation of aqueous solutions, colloidal synthesis, and decomposition of a Pd precursor on Ni particle surfaces. These studies revealed no clear evidence for either strains of Pd surface atoms or core-shell structure. Moreover, only a few papers mention Pd activities for buta-1,3-diene hydrogenation [18,23,24]. Faudon et al. [18] prepared alloyed PdNi nanoparticles by co-impregnating two metallic solutions. The bimetallic particle size was about 2–3 nm; $Pd_{21}Ni_{79}$ and $Pd_{71}Ni_{29}$ particles exposed 53 and 91% of Pd atoms in the outer surface, respectively [18,24]. TOF of $Pd_{21}Ni_{79}$ particles for gas-phase buta-1,3-diene hydrogenation was 5 times lower than for Pd atoms in monometallic particles, whereas the Pd activity for $Pd_{71}Ni_{29}$ particles was close to that for pure Pd. PdNi nanoparticles were also prepared by decomposing Pd precursor on Ni particle surfaces [18,24]; larger particles were obtained (∼7 nm). Pd activity was still lower than that of monometallic Pd particles for buta-1,3-diene hydrogenation. Other studies focused on other reactions such as CO oxidation [20,21,25–27] or nitrobenzene hydrogenation [22,28–30]; only a few clearly showed core–shell structure of NiPd particles [19,20,22]. For nitrobenzene hydrogenation, core–shell NiPd particles are more active than Pd monometallic ones. This is due not to strain effects, but rather to co-existence at the surface of Pd and Ni atoms [30].

To conclude, strained Pd on Ni(110) single crystals is highly active for gas-phase buta-1,3-diene hydrogenation. This activity amplification of Pd atoms is understood as a consequence of strained Pd surface atoms and/or Pd surface reconstruction. Nevertheless, neither Pd activity amplification for buta-1,3-diene hydrogenation nor strains on Pd surface atoms were observed for PdNi three-dimensional supported nanoparticles.

In this paper, we focus on the preparation of core–shell NiPd particles supported on alumina. Such preparation methods as decomposition of a Pd organic precursor on supported Ni particles or preparation of colloidal core–shell bimetallic particles were used to promote core–shell structure formation. Catalysts were then characterized and buta-1,3-diene hydrogenation under liquid-phase conditions was studied.

2. Experimental

2.1. Synthesis of monometallic and bimetallic catalysts

Two different preparation methods for core–shell NiPd bimetallic nanoparticles were investigated. Method 1 was a two-step process involving first preparing supported Ni particles and then decomposing Pd precursor through surface organometallic chemistry [18,20,31,32]. Nickel hydroxide nanoparticles were first synthesized by neutralizing nickel nitrate solution ($Ni(NO_3)_2{\cdot}(H_2O)_6$, 90 mL, [Ni] = 4.5×10^{-2} mol L^{-1}, Fluka, purity 98%) with sodium hydroxide solution (NaOH, 10 mL, 5 mol L^{-1}, VWR Prolabo). The mixture was stirred and immediately impregnated onto 20 g of alumina support (γ-alumina, 127 $m^2\ g^{-1}$, 1.05 $cm^3\ g^{-1}$), and then dried for 12 h at 120 °C under atmospheric conditions. Supported nickel hydroxide nanoparticles were reduced under hydrogen flow for 2 h at 450 °C. Reduced Ni catalyst was then immersed in toluene (100 mL, VWR Prolabo, purity 99.99%) under argon bubbling. Acetylacetone used as an competitor to avoid Pd deposition on alumina (310 mg, AcacH, VWR Prolabo, purity 99.9%), was added to the mixture under hydrogen bubbling (90 mL min^{-1}) for 1 h. Then hydrogen bubbling was stopped, and a 50-mL palladium(II) acetylacetonate solution was added ($[Pd(acac)_2] = 8.2 \times 10^{-3}$ mol L^{-1}, STREM Chemicals, purity 99%). $Pd(acac)_2$ consumption during reaction was followed by UV–visible analyses. The reaction time was about 20 min. Finally, catalyst was washed three times with 150 mL of toluene and dried at 120 °C under atmospheric conditions for 12 h to achieve the bimetallic catalyst.

Method 2 involved the preparation of core–shell bimetallic particles in solution and then supporting them by incipient wetness impregnation on γ-alumina. First, Ni particles were obtained by reducing nickel(II) acetylacetonate anhydrous [536 mg, $Ni(acac)_2$, STREM Chemicals, purity 95%] in ethanol (50 mL, SDS, purity 99%, synthesis grade) by sodium boro-

Table 1
Physico-chemical characteristics of supported catalyst

Catalysts	Ni	Method 1		Method 2		Pd
	A	B	C	D	F	G
Ni (wt%)	1.18	1.21	1.26	1.26	0.33	0
Pd (wt%)	0	0.08	0.13	0.05	0.1	0.25
Ni dispersion (%)	9	/	9	/	/	/
Pd dispersion (200 °C) (%)	/	100	72	73	70	70
Pd dispersion (500 °C) (%)	/	97	87	97	/	47

hydride (414 mg, $NaBH_4$, VWR Prolabo). The stirred green solution of $Ni(acac)_2$ turns to black with the addition of $NaBH_4$ solution. Then a 150-mL palladium acetylacetonate solution was added to the mixture ($[Pd(acac)_2] = 2.3 \times 10^{-3}$ mol L^{-1}). Finally, the solution was impregnated on the alumina support by successive wetness impregnations and dried at 120 °C under atmospheric conditions.

Monometallic reference Pd and Ni catalysts were also prepared. Nickel nitrate solution was reacted with sodium hydroxide similar to step 1 of method 1. Then nickel hydroxide nanoparticles were impregnated on the γ-alumina, dried at 120 °C under atmospheric conditions, and reduced at 450 °C under hydrogen flow for 2 h. Pd catalyst was prepared by decomposing $Pd(acac)_2$ on the γ-alumina. First, γ-alumina was treated at 450 °C under hydrogen flow (2 h) to have the same surface state as alumina from bimetallic catalysts. Then it was immersed in toluene (100 mL) under hydrogen bubbling (90 mL min^{-1}). While hydrogen flow was stopped, a $Pd(acac)_2$ solution (4.5×10^{-3} mol L^{-1}) was added. Finally, the catalyst was washed three times with toluene and dried at 120 °C for 12 h.

Catalysts A and G (Table 1) are Ni and Pd reference catalysts. Catalysts B, C, and D are the bimetallic catalysts prepared following method 1. Catalysts E (unsupported catalyst) and F (supported catalyst) are prepared following method 2.

2.2. Characterisation

The chemical composition of catalysts was measured by X-ray fluorescence (Ni) and atomic adsorption (Pd). UV–visible spectroscopy was performed on an ELMER LAMBDA 11 UV/vis spectrometer. Solutions were analysed in 1-mm-thick quartz cells. UV–vis measurements were made to evaluate $Pd(acac)_2$ consumption with time following step 2 of method 1.

Metal accessibility was measured by performing O_2 chemisorption on a X-Sorb@ apparatus. Metallic dispersion of each metal (Pd, Ni) or both in combination (Pd + Ni) was determined by measuring oxygen consumption during the oxidization of the metallic particle surfaces previously reduced at different temperatures. In that sense, a first reduction step at 200 or 500 °C was applied to ensure that Pd is fully reduced and to release acacH ligands from synthesis still adsorbed on catalyst particles. A return to room temperature was effected under helium flow. After 1 h at 30 °C under helium, O_2 pulses were operated and O_2 consumption was measured. After these pretreatments, two different reduction steps were performed: reduction at 30 °C to reduce only Pd and reduction at 500 °C to reduce Pd and Ni. After each reduction, return to temperature was also performed under helium flow and O_2 consumption was determined. Pd and Ni dispersion was thus calculated based on the ratio between adsorbed oxygen atoms and metallic atoms

$$\mathrm{Ni} + (1/2)\mathrm{O_2} \rightarrow \mathrm{NiO}, \quad \mathrm{Pd} + (1/2)\mathrm{O_2} \rightarrow \mathrm{PdO},$$

$$D = \frac{V_a \times M_M}{\%_M \times V_m \times \chi}, \tag{1}$$

where V_a is adsorbed oxygen volume (mL g^{-1}), M_M—molar weight of metal (g mol^{-1}), V_m—molar volume (24666 cm^3 at 25 °C), χ—stoichiometric coefficient $O_2/M = 1/2$, $\%_M$—metallic weight.

Temperature-programmed reduction (TPR) was performed using an Autochem II device (Micromiretics). Catalysts were first calcined at 200 °C under oxygen flow, then reduced during TPR under hydrogen flow from 30 to 1000 °C (heating rate 5 °C/min).

TEM observations were obtained using a Philips Tecnai microscope, working at 200 kV, with a spatial resolution of 0.19 nm and a detection limit of 0.7 nm. Samples were put onto a copper microgrid. The average size of metallic particles was estimated by counting 200 particles on TEM micrographs and making an arithmetic average,

$$d_{moy} = \frac{\sum_n n d_n}{n}, \tag{2}$$

where d_{moy} is average particle size (nm), d_n—particles size measured by TEM (nm), n—particles number. The chemical composition of particles was determined by EDX analyses. Accuracy of EDX measurements on the number of detected bimetallic particles was 95%. Experimental results were compared with expected values using a layer-by-layer model assuming a core–shell structure for bimetallic particles. Following Van Hardeveld and Hartog's model [34], bimetallic particles were modeled as cubo-octahedra. Starting from a given particle size, we first assumed a Pd surface/Ni surface stoichiometry of 1. The Pd/Ni molar ratios as a function of the particle size, for various Pd coverages (expressed in layers), are reported and compared with Pd/Ni ratios determined experimentally in Fig. 1.

To determine the in-depth location of the metallic particles in the support grains, electron probe microanalyses were done using a CAMECA SX100 electron microprobe microanalyser (acceleration tension, 200 kV; current, 200 nA; TAP crystals, LLIF for Ni analyses [K_α] and LPET for Pd analyses [L_α]). Counting time was nearly 40 s, and a variable step was applied, every 5 μm in the grain edge (300 μm deep) and every 100 μm in the grain core.

XPS measurements were performed on a KRATOS Axis Ultra spectrometer using a monochromatic AlK_α radiation ($h\nu$ = 1486.6 eV). Catalysts were reduced in situ under hydrogen flow before XPS measurements at 200 °C for bimetallic catalysts and at 500 °C for catalyst G. A higher reduction temperature was used for the monometallic Pd catalyst to decrease Pd dispersion in order to obtain a particle size close to that of the bimetallic catalysts. Experiments were made under secondary

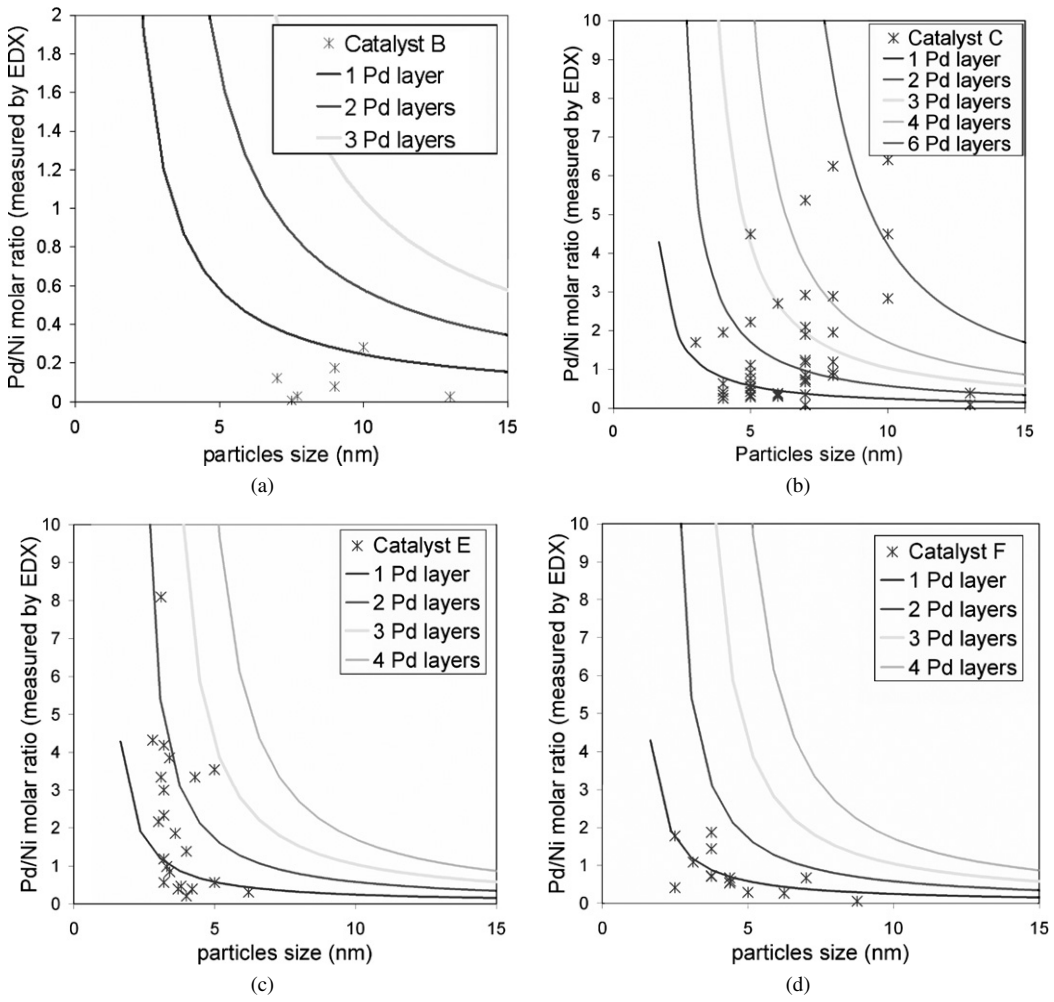

Fig. 1. PdNi bimetallic nanoparticles composition characterized by EDX: catalysts B (a), C (b), E (c) and F (d).

vacuum ($<10^{-9}$ mbar); the resolution was about 0.7 eV. Spectra were calibrated using the C_{1s} core level associated with carbon pollution on the alumina support at 284.6 eV as a reference. Photo peak decompositions were made using asymmetric and Gaussian–Lorentzian-type curves.

EXAFS experiments were carried out at the X1 beam line of the HASYLAB facility (Hamburg, Germany) using the synchrotron radiation from the DORIS III ring running at 4.45 GeV (with positrons) with an average current of 120 mA. The Pd K-edge at 24.350 eV was monitored in the transmission mode, using a double Si(311) crystal monochromator (detuned to 70% of the primary intensity to eliminate higher orders of diffraction in the transmitted beam) and three ion chambers as detectors (measuring intensity before and after the sample and a reference sample). EXAFS measurements were performed only at the Pd K-edge. In the case of Ni (core)–Pd (shell) particles, informations obtained at the Ni K-edge would not be useful to characterize a Pd shell because EXAFS is a global analysis. The signal-to-noise ratio was optimised by acquiring multiple scans for each spectrum. The total acquisition time was varied depending on the Pd concentration in the catalyst. To characterize the Pd environment evolution during reduction treatments, a cell for in situ measurements was used. The cell was heated in an oven and crossed by the X-ray beam, while nitrogen or hydrogen flows were maintained to keep the catalyst in the same state as during the reduction procedure used to activate the catalysts before catalytic reactions. EXAFS measurements were obtained during the reduction treatment.

EXAFS analysis was performed using the Athena-Artemis software package [35] as described previously [36]. Cubic splines were used to obtain a smooth atomic background and to extract the EXAFS function. The radial distribution function was calculated by Fourier transform of the k-weighted experimental EXAFS function, multiplied by a Hanning window into the R space. EXAFS data analysis was performed using theoretical backscattering phases and amplitudes calculated with code FEFF6 [37].

2.3. Catalytic reaction

Before catalytic reactions, catalysts were reduced at different temperatures under hydrogen gas flow. Buta-1,3-diene selective hydrogenation reactions were performed in liquid phase using a laboratory-scale stainless-steel and perfectly stirred batch reactor (525 mL) working under static conditions, that is, with variation of the concentration of the reactants and products over

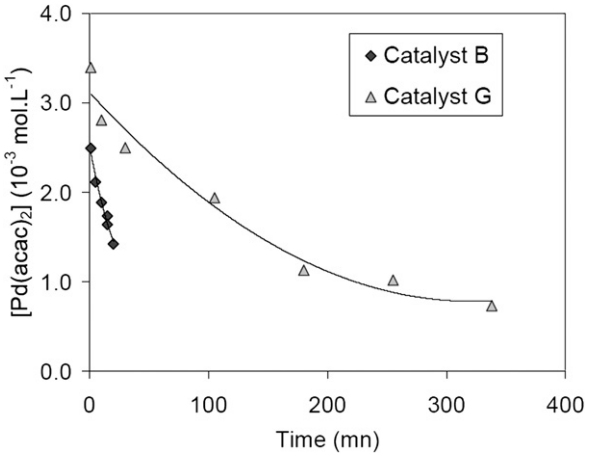

Fig. 2. Concentration of $Pd(acac)_2$ as function of time along Pd deposits for catalysts B and G.

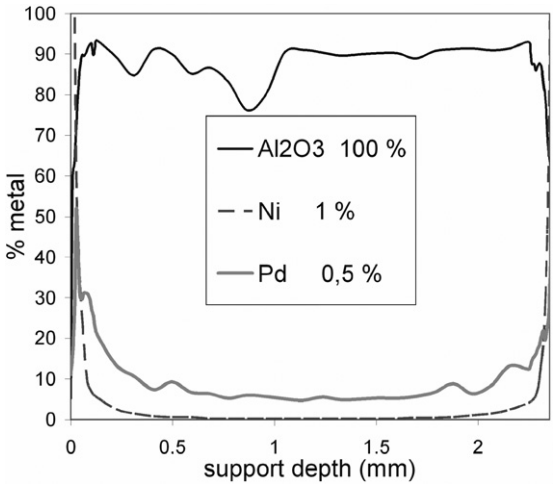

Fig. 3. Metallic repartition profile and molar Pd/Ni ratios for catalyst B as a function of support depth (measured by electron probe microanalysis).

time. Approximately 0.5 g of prereduced catalyst was put in contact with buta-1,3-diene (nearly 7 g) diluted in 240 mL of *n*-heptane, at 5 °C and under 5 bars of H_2, with a high stirring velocity (1600 turns/min). Experimental conditions were previously selected to avoid mass transfer limitations. The reacting mixture is sampled over time and analysed by a gas chromatograph equipped with a plot alumina column (PONA $L = 50$ m, split injector) and a flame ionization detector (at 350 °C).

3. Results

3.1. Pd deposition followed by UV–visible spectroscopy

Pd precursor consumption during the Pd deposit step in method 1 was followed by UV–vis spectroscopy. The evolution of concentrations of $Pd(acac)_2$ with time in the solution are plotted in Fig. 2. Consumption of $Pd(acac)_2$ for catalyst B (i.e., on alumina-supported Ni particles) was faster than deposition of Pd on alumina (catalyst G). The decomposition of $Pd(acac)_2$ follows a first order reaction with respect to reactant. For catalysts B and G, the reaction rate constants were 4.6×10^{-4} s^{-1} and 0.7×10^{-4} s^{-1}, respectively.

3.2. Macroscopic characterisation of catalysts

Chemical compositions and metallic dispersions of catalysts A, B, C, D, F, and G are listed in Table 1. Pd dispersions of bimetallic catalysts were >70%. For all bimetallic catalysts, even if Ni was present all along the support grain, Pd and Ni were present together for the most part in the same area at the edge of the support grain, as shown by electron probe microanalysis; see, for example, the metallic repartitions of catalyst B plotted in Fig. 3.

TPR profiles of catalysts A, C, and G were measured after calcination at 200 °C. A reduction peak centred near 420 °C can be seen in the TPR profile for the Ni catalyst A (Fig. 4). The TPR profile of Pd catalyst G shows a broad and weak reduction peak at 420 °C, which may be consistent with the decomposition and release of acacH still present on the catalyst [33]. The

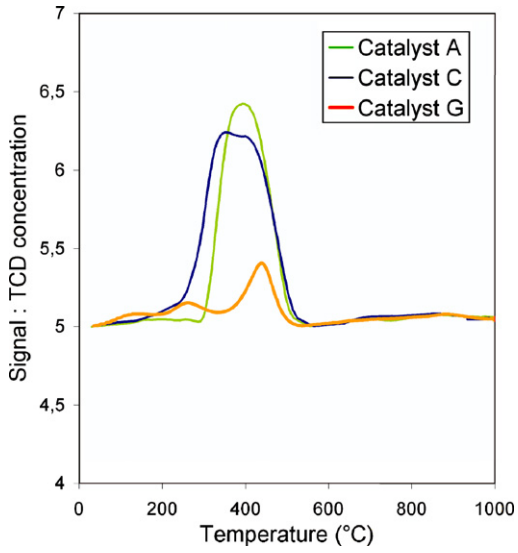

Fig. 4. TPR profiles of catalysts A, C and G.

TPR profile of the bimetallic PdNi catalyst C shows a reduction peak at a lower temperature (390 °C) than that observed for catalysts A and G. Thus, according to literature, the addition of Pd atoms at the surface of Ni particles should decrease the Ni reduction temperature [18].

XPS peaks corresponding to metallic $Pd_{3d_{5/2}}$ core electrons energy (around 335.0 eV) can be divided into three subpeaks: 334.4 eV (surface Pd atoms), 335.0 eV (bulk Pd atoms), and 335.5 eV (surface Pd atoms linked to oxygen or hydrogen atoms) as described previously [38,39]. The main contribution of Pd core electron energy has a lower value (334.4 eV) for both bimetallic catalysts C and F than for the monometallic catalyst G (335.5 eV) used as a reference (Table 2). This low $Pd_{3d_{5/2}}$ electron energy value of 334.4 eV for core–shell NiPd particles contradicts previous values measured on PdNi model catalysts that revealed an increase of the Pd core electron energy of up to 0.5 eV. Nevertheless, this value of 334.4 eV is consistent with the presence of a Ni (core)–Pd (shell) structured particle

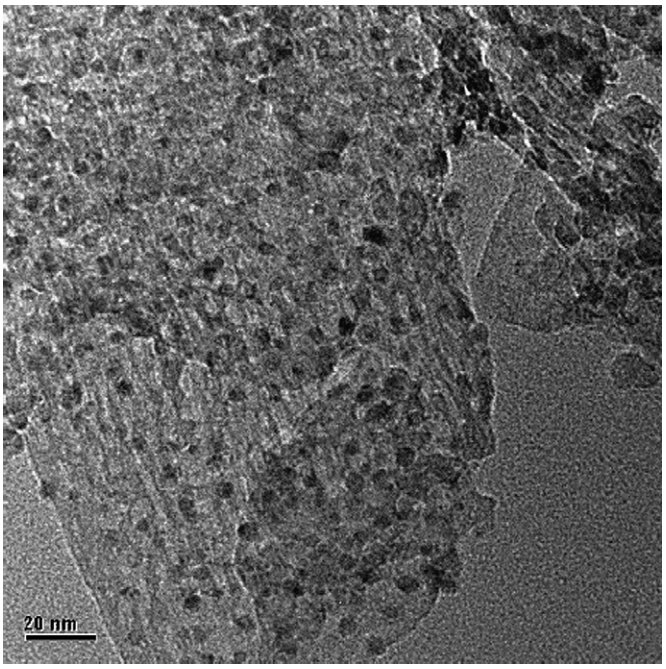

Fig. 5. TEM micrograph of nanoparticles of catalyst C.

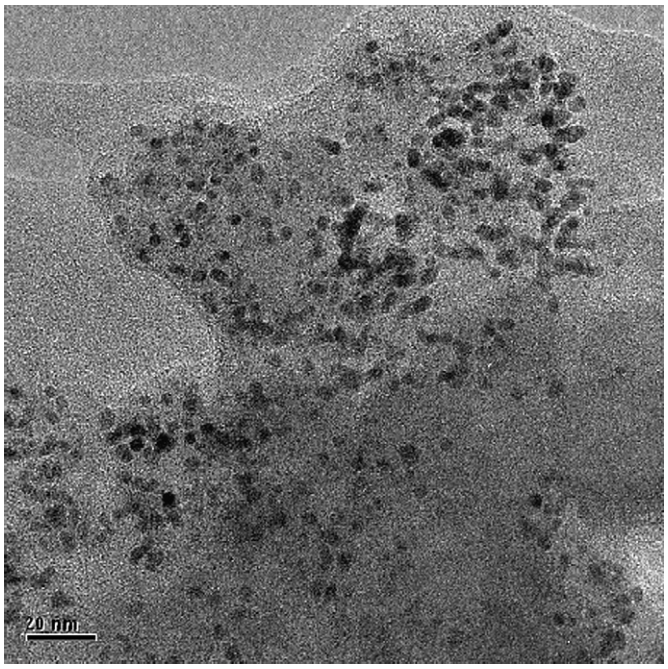

Fig. 6. TEM micrograph of nanoparticles of catalyst E.

with a single layer of uncoordinated Pd present on Ni particle surface [40]. It also could be induced by electronic effects between Ni (Pauling electronegativity = 1.8) and Pd (Pauling electronegativity = 2.2) in contact.

3.3. Nanoscale characterization of catalysts

3.3.1. Particle sizes of PdNi bimetallic nanoparticles

TEM micrographs of catalysts C and E are shown in Figs. 5 and 6, respectively. Particle size distributions were determined from TEM analysis of the bimetallic catalysts B, C, and F (Fig. 7). The particle size of catalysts B and C ranged between 3 and 20 nm (Fig. 7), with average sizes of 6.2 mm for catalyst B and 7.2 mm for catalyst C. Moreover, large aggregates (>100 nm) were also observed on both catalysts. The average particle diameter of catalyst F was 4.5 nm with a quite narrow particle size range of 2–8 nm (Fig. 7). Following synthesis method 2, many particles are agglomerated on the support, but each particle seems to keep its primary morphology. These aggregates are quite large (200 nm).

3.3.2. Bimetallicity of PdNi particles

The first metallic repartition profile shows that for each bimetallic catalysts, Pd and Ni were mainly located in the same area of the support (Fig. 3). Information on particle bimetal-

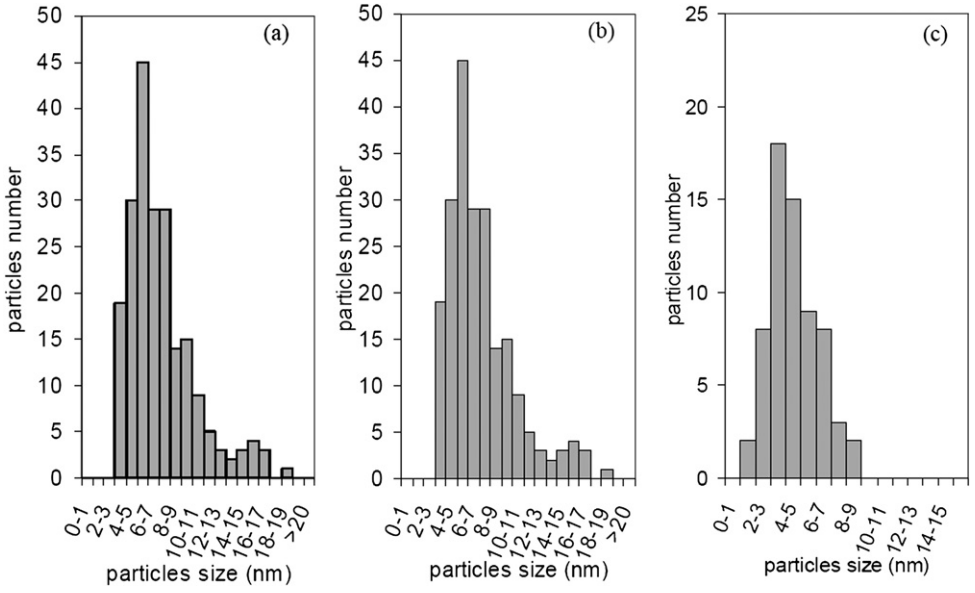

Fig. 7. Size repartition of nanoparticles of catalysts B (a), C (b) and F (c).

Table 2
Pd core electrons energy measurements: subpeaks contributions (%) for catalysts C, F and G

Pd core electrons energy (eV)	Subpeaks contributions (%)		
	Catalyst		
	C	F	G
334.4 ± 0.2	70	63	10
335.5 ± 0.2	17	18	68
336.8 ± 0.2	13	19	22

Table 3
Percentages of bimetallic particles observed on catalysts B, C, E and F (from EDX measurements) and percentages of bimetallic particles assuming a core–shell structure with less than 1 or 2 Pd surface layers

EDX measurement on nanoparticles	Catalyst			
	B	C	E	F
% of bimetallic particles	33	87	96	78
% of particles with Pd coverage				
<1 Pd layer	100	47	45	75
<2 Pd layers	0	60	86	100

licity can be obtained from EDX measurements. Experimental Pd/Ni molar ratios are plotted in Fig. 1 as function of particles size for catalysts B, C, E, and F. Theoretical Pd/Ni molar ratios for 1, 2, 3, 4 and 6 Pd layers on Ni particles are also reported. For catalysts B and C prepared following method 1, only Ni monometallic and PdNi bimetallic particles were observed; no Pd monometallic particles were detected. In catalysts B and C, 33% and 87% of the analysed particles, were bimetallic, respectively (Table 3). The Pd coverage for catalyst B should be considered lower or equal to 1 layer for all particles. Catalyst C had the highest Pd coverage, with 60% of bimetallic particles coverage lower than 2 Pd layers deposited on Ni particles. Consequently, for 40% of the bimetallic particles of catalyst C, Pd coverage was greater than 2 Pd layers on Ni particles. Catalysts E and F prepared following method 2 had Pd coverage less than 2 Pd layers deposited on Ni particles (Table 3).

3.3.3. Core–shell structure of NiPd particles and strained Pd observed by EXAFS

Catalysts B, C, and F were analysed by EXAFS at the Pd *K*-edge. According to Fourier-transformed EXAFS functions, the evolution of the Pd–Pd and Pd–Ni bond lengths for various reduction temperatures are shown in Fig. 8. The numbers of Pd and Ni neighbours to Pd for catalysts B, C, and F are given in Table 4.

Up to a reduction temperature of 200 °C, each Pd atom for catalysts B and C had nearly 6 Pd atoms and 2 Ni atoms as nearest neighbours (Table 4). This is in agreement with the presence of bimetallic particles. Indeed, for large isolated monometallic Pd particles, the Pd neighbourhood would be composed of almost 12 Pd atoms and no Ni atoms, whereas the NiPd core–shell structure would have 6 Pd atoms and 3 Ni atoms as nearest neighbours for the Pd surface atoms [for the (111) face]. Therefore, the average structure can be proposed to be a core–shell one.

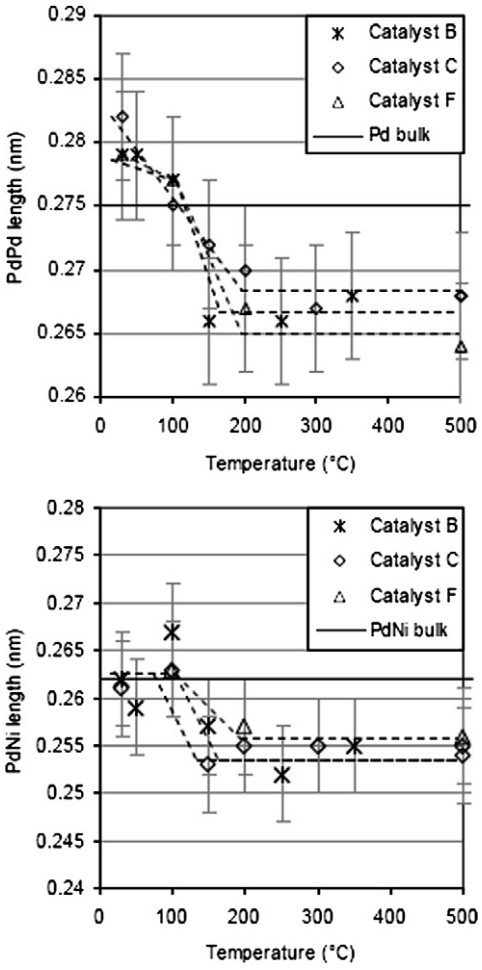

Fig. 8. Pd–Pd and Pd–Ni length evolutions during the reduction procedure for catalysts B, C and F (measured by EXAFS).

A similar conclusion can be drawn by analysing the EXAFS data of catalyst F. This catalyst is also composed of bimetallic particles. The Pd neighbourhood was more than 6 Pd atoms and less than 2 Ni atoms (Table 4). This is in agreement with a core–shell structure corresponding to a Pd coverage close to 1 monolayer.

For both catalysts, the core–shell structure of the bimetallic particles was quite stable until 300 °C. After reduction at 500 °C, the number of Pd nearest neighbours of Pd atoms decreased while the number of Ni neighbours increased. This could be in agreement with Pd surface atoms diffusing slowly into the bulk of the particles composed of Ni. Nevertheless, the mean value of the number of nearest neighbours of Pd atoms (Pd + Ni) was still much less than 12 (actually nearly 8) after reduction at 500 °C. Even if Pd and Ni atoms were mixed at 500 °C, most of the Pd atoms still remained at the particle surface also according to chemisorption measurements, which showed Pd dispersions close to 100% after pretreatment reduction at 500 °C (Table 1).

Moreover, the Pd–Pd bond length decreased while the reduction temperature increased. Pd–Pd length ranged from 0.280 nm (±0.005 nm) at room temperature to nearly 0.265 nm (±0.005 nm) for reduction temperatures above 200–300 °C

Table 4
Number of Pd and Ni neighbours to Pd atoms for catalysts B, C and F determined from EXAFS data

Temperature (°C)	Catalyst					
	B		C		F	
	Ni neighbours number to Pd	Pd neighbours number to Pd	Ni neighbours number to Pd	Pd neighbours number to Pd	Ni neighbours number to Pd	Pd neighbours number to Pd
30	2.6 (±1.3)	4.2 (±1.0)	2.3 (±0.9)	4.8 (±1.1)		5.6 (±0.8)
50	2.4 (±1.3)	4.5 (±1.0)				
100	2.9 (±1.5)	4.5 (±1.5)	1.7 (±0.4)	7.8 (±0.8)	1.5 (±0.3)	7.4 (±0.8)
150	2.8 (±1.6)	3.1 (±2.0)	2.0 (±0.6)	5.6 (±0.6)		
200			2.0 (±0.5)	5.9 (±0.8)	2.5 (±0.4)	5.9 (±0.8)
250	2.5 (±1.6)	2.3 (±2.0)				
300			2.4 (±0.4)	5.5 (±0.7)		
350	2.2 (±1.6)	4.1 (±2.0)				
500			4.1 (±0.3)	3.9 (±0.7)	4.6 (±0.4)	3.5 (±0.5)

(Fig. 8). Simultaneously, the Pd–Ni bond length varied from 0.263 nm (±0.005 nm) at room temperature to 0.255 nm (±0.005 nm) for reduction temperatures above 200 °C. Such a value was greater than that from pure Ni bulk (Ni–Ni length, 0.249 nm) and corresponds to the expected value for a Pd–Ni bulk alloy with 23 at% of Pd content considering Veggard's law. Those results highlight a compressive strain on Pd surface atoms of bimetallic particles of catalysts B, C, and F, which is consistent with compression observed on bimetallic PdNi extended surfaces [14].

3.4. Catalytic properties for buta-1,3-diene hydrogenation in liquid-phase conditions

Before reactions, specific reduction treatments under hydrogen flow were realised on catalysts at 30, 200, and 500 °C. Those temperatures correspond to particular states of Pd surface atoms. At 30 °C, Pd surface atoms on bimetallic catalysts suffer a tensile strain and interact with residual acacH ligands as shown by EXAFS and TPR. At 200 °C, Pd surface atoms suffer a compressive strain with acacH probably still present on the catalyst as shown by TPR and chemisorption measurements. Nevertheless, metal accessibilities used to calculate TOF were also determined after pretreament under hydrogen at 200 °C. At 500 °C, in addition to compressive strains, Pd surface atoms started alloying with Ni atoms.

Hydrogenation reaction rates and TOF (moles of buta-1,3-diene converted per accessible Pd surface atom determined by chemisorption measurements) are reported in Table 5. The reaction rate was lower for the Ni reference catalyst (A) than for any Pd monometallic or bimetallic catalysts; consequently, the activity of the Ni particles was in our conditions negligible compared to surface atom of Pd or NiPd particles. For the Pd reference catalyst (G), the reaction rate increased until a reduction temperature of 200 °C. The reaction rate of catalyst G then decreased, but TOF increased, with increasing reduction temperature. This may be related to variations in Pd dispersion. Indeed, the Pd dispersion of catalyst G was 70% after reduction at 200 °C and decreased to 47% after reduction at 500 °C, due to sintering phenomena (Table 1). Even if reaction rates and TOF of bimetallic catalysts were variable, they were nearly 10 times lower than those of catalyst G.

Table 5
Reaction rates and TOFs of catalysts A, C, D, F and G for buta-1,3-diene hydrogenation

Reduction treatment temperature (°C)	Catalyst				
	A	C	D	F	G
Reaction rates (mol mm^{-1} g_{Pd}^{-1}) (±5%)					
30		0.3	1.8	2.6	0.3
200		2.6	3.2	2.0	28.4
500	0.01[a]	0.5	6.4	0.2	24.9
TOFs (s^{-1}) (±5%)					
30		0.8	4.4	6.7	0.6
200		6.6	7.8	3.1	68.4
500	0.07[a]	1.2	15.8		93.8

[a] Reaction rate and TOF for catalyst A were calculated respectively per nickel weigh and nickel surface atom instead of palladium ones.

4. Discussion

4.1. Bimetallicity of PdNi particles

Following method 1, the average size of the PdNi particles was 6–7 nm (Fig. 7). As shown by UV–vis measurements, Pd precursor consumption showed that the reaction was more rapid in the presence of supported Ni particles compared with Pd deposition on alumina, highlighting the interaction between Ni nanoparticles and Pd precursor. We also found evidence that Pd and Ni were macroscopically located together for the most part at the edge of the support grain.

According to EDX analyses for both B and C catalysts, all Pd atoms were apparently in contact only with Ni particles; no monometallic Pd particles were detected on the support. Moreover, Pd coverage of bimetallic particles was close to 1 Pd layer (Table 3).

TEM analyses showed that PdNi bimetallic particles size prepared following method 2 were centred around 4.5 nm. Pd and Ni atoms of the supported catalyst F were located at the edge of the support grain. For catalysts E and F, the Pd/Ni molar ratios were for the most part close to that expected for 1 Pd layer on Ni particles.

The bimetallic catalysts prepared by both methods showed bimetallic particles and no monometallic Pd particles. Moreover, the Pd–Ni molar ratios measured on those bimetallic cat-

alysts were in accordance with those calculated for core–shell NiPd particles with 1 or 2 Pd layers even if the core–shell structure was not yet apparent.

4.2. Core–shell structure of particles

For both preparation methods, Pd dispersion of catalysts measured after pretreatment at 200 °C was >70%, implying that Pd was accessible mainly at the surface of bimetallic particles (Table 1). TPR analysis (Fig. 4) showed decomposition of residual acacH ligand for temperatures close to 400 °C. Dispersions of 70% measured after pretreatment at 200 °C were consistent with the presence of residual acacH on the catalyst. Moreover, dispersions measured after pretreatment at 500 °C, and thus with elimination of acacH, were close to 100%. XPS analyses of C and F catalysts (Table 2) showed a significant contribution of the subpeak at 334.4 eV relevant for surface uncoordinated Pd atoms [40]. Contributions at 335.5 eV (bulk Pd atoms) and 336.8 eV (oxidized Pd atoms) for catalysts C and F were negligible. All of these observations were relevant for a bimetallic core–shell structure.

Moreover, according to EXAFS measurements (Table 4), at reduction temperatures up to 300 °C, the Pd neighbourhoods of catalysts B, C, and F were close to those expected for 1 Pd layer on Ni particles. According to the number of nearest neighbours deduced from EXAFS data and the Pd dispersion measured by chemisorption, Pd atoms were located at the surface of bimetallic particles. At temperatures above 300 °C, the number of Pd and Ni neighbours of Pd atoms decreased and increased, respectively, which may be ascribed to alloy formation. Nevertheless, the global number of neighbours remained quite constant (nearly 8). So Pd and Ni atoms mixed, but Pd atoms remained mainly on the top surface.

In conclusion, prepared bimetallic particles showed a core–shell structure with Pd atoms located on the particles surface.

4.3. Strains on Pd surface atoms of bimetallic particles

EXAFS analyses showed evidence of strained Pd. For catalysts B, C, and F, the Pd–Pd lengths decreased from 0.280 nm to nearly 0.265 nm while the reduction temperature was varied from 30 to 200 °C (Fig. 8).

At 200 °C, the Pd–Pd length was greater than expected for a topotactic growth of the Pd layer on pure Ni (Ni–Ni length, 0.249 nm). This length was less than that for Pd bulk (0.275 nm), indicating compressive strain on surface Pd atoms. This measurement is in accordance with previous ones on single crystals [14]. Moreover, the Pd–Pd length was equal to the average Pd–Pd and Ni–Ni lengths for pure metals. This phenomena has been observed for other bimetallic systems as well [40,41]. Note that the Pd–Ni length (0.255 nm) was less than the sum of the atomic radii of Pd^0 and Ni^0 atoms (0.262 nm) associated with contraction of Pd surface atoms (Fig. 8).

Surprisingly, at 30 °C under hydrogen flow, the Pd–Pd length was greater than that for bulk Pd. Keeping in mind that EXAFS results showed that Pd was fully reduced even at 30 °C, we can suggest that Pd was on oxidized Ni. The Ni–Ni length in NiO was 0.294 nm, and the Pd–Pd length (0.280 nm) was between the Pd–Pd and Ni–Ni lengths of pure Pd and NiO crystals (Table 6). Thus, at 30 °C Pd surface atoms sustained some tensile strain.

Table 6
Pd, PdNi, NiO and Ni crystal structure parameters

	Structure	Lattice parameter (Å)	M–M length (Å)
Pd	FCC	3.89	2.75
PdNi	Solid solution	3.69	2.61
NiO	FCC (NaCl structure type)	4.16	2.94
Ni	FCC	3.52	2.48

XPS core electron energies of C and F catalysts reduced at 200 °C were lower than those expected for bulk Pd. In contrast, an increase in the Pd core electron energy of about 0.5 eV (to 335.5 eV) was measured for Pd on Ni crystals for which Pd retained compressive strains [5]. However, reconstructions occurred on extended surfaces, which may not have been the case for small particles. Nevertheless, it is known that compressive strains induced an increase of the d-band width, which would be expected to lead to a downshift in the gravity centre of the d-band, that is, toward higher binding energy [10]. XPS results on Pd deposit on Ni crystals were in agreement with the compressive strain effect. In contrast, for one Pd layer on 5 nm NiPd core–shell particles, XPS results showed an up-shift toward lower binding energy of the gravity centre of the d-band of Pd atoms. This lower binding energy of surface Pd atoms can be ascribed to direct electronic effects between Ni and Pd in contact, because Pd is more electronegative than Ni (Paulings electronegativity, 2.2 for Pd and 1.8 for Ni). This also may be in accordance with Pd decoordination effects [42]. These two phenomena should appear as a first-order electronic effect compared with the compressive strain induced on Pd–Pd bonds for PdNi-supported particles.

4.4. Catalytic performance

After reduction at 200 °C, all catalytic activities of the PdNi bimetallic catalysts were lower than that of the monometallic Pd catalyst, even when a compressive strain was evidenced on Pd atoms (Fig. 9). The TOF of Pd surface atoms measured for bimetallic particles was 10 times lower than for Pd monometallic catalyst. These results are in accordance with previous findings obtained on bimetallic particles [18,23,24]. Because core–shell structure and compressive strains on Pd atoms were seen on our bimetallic catalysts, we can assume that the Pd activity amplification observed on PdNi bimetallic extended surfaces [1,14] was not observed on 5 nm supported PdNi particles. This may be due to a particle size effect or to an electronic effect. Indeed, it has been shown that reconstructions occur on the Pd surface of PdNi single crystals; periodically, one Pd atom seems to leave the row and create new original active sites with low-coordinated Pd atoms [14,17]. The geometric periodicity was rather long (every 5–11 atomic distances); therefore, the exposed nanofacets present on 5 nm particles may be too small

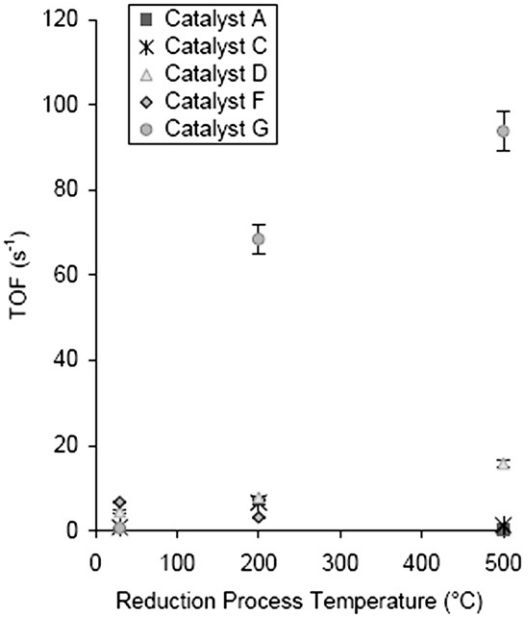

Fig. 9. Bimetallic and monometallic catalysts TOFs versus reduction process temperature.

to allow this to happen. Concerning the possibility of an electronic effect, we found that the compressive strain of Pd–Pd bonds induced an increase in Pd binding energy in the case of extended-surface catalysts. For PdNi-supported particles, the lower binding energy of Pd should correspond to electronic or uncoordinated Pd effects.

5. Conclusion

Core–shell supported NiPd bimetallic nanoparticles were synthesized following two chemical methods. The average particle size obtained for PdNi nanoparticles was about 5–6 nm. For all catalysts, Pd coverage was nearly 1 or 2 layers. Previously, PdNi model catalysts have shown Pd reaction rate amplification for buta-1,3-diene selective hydrogenation in a similar Pd coverage range (from 1 to 4 layers). This effect can be explained by compressive strains on Pd surface atoms and/or geometric partial relaxation without clear evidence of their respective impact.

According to EXAFS analyses, compressive strain on Pd was evidenced on 5 nm PdNi bimetallic particles. However, no reaction rate amplification of Pd was obtained with those catalysts, and the strained Pd TOF was 10 times lower than that for pure Pd catalysts. These results indicate that Pd activity amplification observed on model catalyst may be preferentially due to surface reconstruction as row Pd structures evidenced by surface X-ray diffraction [17] rather than a compressive strain on Pd surface atoms. This surface reconstruction cannot occur on 5 nm supported PdNi particles because of the presence of a high proportion of unsatured atoms. In addition, electronic effects were also detected. The critical size that allows surface reconstructions should be determined. Because 1 Pd atom is out of the crystal every 5–10 Pd atoms in a row, the particle size must be large enough to expose surfaces that are long enough to develop surface reconstructions. Work is in progress to determine this particle size and to study its influence on strain and electronic effects on supported bimetallic particles.

Acknowledgment

The authors thank the IFP Physics & Analysis Department for carrying out the various characterization experiments and helping to interpret the results.

References

[1] J.C. Bertolini, Y. Jugnet, in: D.P. Woodruff (Ed.), Alloy Surfaces and Surface Alloys, vol. 10, Elsevier, Amsterdam, 2002, pp. 404–437.
[2] J.H. Sinfelt, J.L. Carter, J.C. Yates, J. Catal. 24 (1972) 283.
[3] G.A. Martin, Catal. Rev. Sci. Eng. 30 (1988) 519.
[4] T.M. Tri, J. Massardier, P. Gallezot, B. Imelik, J. Catal. 85 (1984) 244.
[5] J.C. Bertolini, P. Miegge, P. Hermann, J.L. Rousset, B. Tardy, Surf. Sci. 331–333 (1995) 651.
[6] S. Helfensteyn, J. Luyten, L. Feyaerts, C. Creemers, Appl. Surf. Sci. 212–213 (2003) 844.
[7] J.L. Rousset, J.C. Bertolini, P. Miegge, Phys. Rev. B 53 (1996) 4947.
[8] P. Miegge, J.L. Rousset, B. Tardy, J. Massardier, J.C. Bertolini, J. Catal. 149 (1994) 404.
[9] A.C. Michel, L. Lianos, J.L. Rousset, P. Delichère, N.S. Prakash, J. Massardier, Y. Jugnet, J.C. Bertolini, Surf. Sci. 416 (1998) 288.
[10] A. Ruban, B. Hammer, P. Soltze, H.L. Skriver, J.K. Norskov, J. Mol. Catal. A 115 (1997) 421.
[11] P. Hermann, D. Simon, P. Sautet, B. Bigot, J. Catal. 167 (1997) 33.
[12] P. Hermann, B. Tardy, D. Simon, J.M. Guigner, B. Bigot, J.C. Bertolini, Surf. Sci. 307–309 (1994) 422.
[13] P. Hermann, J.M. Guigner, B. Tardy, Y. Jugnet, D. Simon, J.C. Bertolini, J. Catal. 163 (1996) 169.
[14] J.S. Filhol, M.C. Saint-Lager, M. De Santis, P. Dolle, D. Simon, R. Baudoing-Savois, J.C. Bertolini, P. Sautet, Phys. Rev. Lett. 89 (2002) 146106-1.
[15] J.S. Filhol, D. Simon, P. Sautet, Surf. Sci. Lett. 472 (2001) L139.
[16] J.C. Bertolini, Appl. Catal. A 191 (1999) 15.
[17] M.C. Saint-Lager, S. Ferrer, C. Walker, O. Robach, A. Bailly, J.C. Bertolini, R. Baudoing-Savois, L. Piccolo, P. Dolle, Y. Jugnet, Surf. Sci. 587 (2005) 229.
[18] J.F. Faudon, F. Senocq, G. Bergeret, B. Moraweck, G. Clugnet, C. Nicot, A. Renouprez, J. Catal. 144 (1993) 460.
[19] S.U. Son, Y. Jang, J. Park, H.B. Na, H.M. Park, H.J. Yun, J. Lee, T. Hyeon, J. Am. Chem. Soc. 126 (2004) 5026.
[20] S. Sao-Joao, S. Giorgio, C. Chapon, S. Bourgeois, C.R. Henry, J. Phys. Chem. B 109 (2005) 342.
[21] V.I. Koval'chuck, N.V. Chesnokov, A.V. Kalinkin, L.V. Naimushina, B.N. Kuznetsov, Kinet. Catal. 36 (1995) 396.
[22] K. Nagaveni, A. Gayen, G.N. Subbanna, M.S. Hedge, J. Mater. Chem. 12 (2002) 3147.
[23] A. Sarkany, Stud. Surf. Sci. Catal. 130 (2000) 2081.
[24] J. Massardier, J.F. Faudon, G. Bergeret, J.L. Rousset, P. Delichère, A. Renouprez, J. Catal. 170 (1997) 181.
[25] A.B. Hungría, N.D. Browning, R.P. Erni, M. Fernández-García, J.C. Conesa, J.A. Pérez-Omil, A. Martínez-Arias, J. Catal. 235 (2005) 251.
[26] A.B. Hungría, M. Fernández-García, J.A. Anderson, A. Martínez-Arias, J. Catal. 235 (2005) 262.
[27] A.B. Hungrý, J.J. Calvino, J.A. Anderson, A. Martínez-Arias, Appl. Catal. B 62 (2006) 359.
[28] P. Lu, T. Teranishi, K. Asakura, M. Miyake, N. Toshima, J. Phys. Chem. B 103 (1999) 9673.
[29] R. Raja, V.B. Golovko, J.M. Thomas, A. Berenguer-Murcia, W. Zhou, S. Xiee, B.F.G. Johnson, Chem. Commun. (2005) 2026.
[30] P. Lu, N. Toshima, Bull. Chem. Soc. Jpn. 73 (2000) 751.

[31] S. Sao-Jao, S. Giorgio, C.R. Henry, J.M. Penisson, ICEM, 2002, p. 417.
[32] S. Sao-Jao, S. Giorgio, C.R. Henry, J.M. Penisson, ICEM, 2002, p. 387.
[33] J. Goetz, R. Touroude, M.A. Volpe, J. Catal. 164 (1996) 369.
[34] R. Van Hardeveld, F. Hartog, Surf. Sci. 15 (1969) 189.
[35] B. Ravel, M. Newville, J. Synch. Rad. 12 (4) (2005) 537.
[36] Y. Iwasawa, X-Ray Absorption Fine Structure for Catalysts and Surfaces, World Scientific, London, 1996.
[37] J.J. Rehr, R.C. Albers, Rev. Mod. Phys. 72 (2000) 621.
[38] D. Teschner, R. Schlögl, Knop-Gericke, H. Sauer, H. Bluhma, M. Hävecker, E. Kleimenov, A. Pestryakova, J. Catal. 230 (2005) 186.
[39] J.N. Anderson, O. Bjôrncholm, A. Sandel, R. Nyholm, J. Forsell, L. Thanell, A. Nilsson, N. Martensson, Synch. Rad. News 4 (1991) 15.
[40] N. Toshima, T. Yonezawab, New J. Chem. (1998) 1179.
[41] O. Robach, H. Isern, P. Steadman, K.F. Peters, C. Quiros, S. Ferrer, Phys. Rev. B 68 (2003) 214416-1.
[42] C. Mottet, G. Tréglia, B. Legrand, Surf. Sci. 352–354 (1996) 375.